ELSEVIER

Chemical Engineering Journal 137 (2008) 137–143

Chemical Engineering Journal

www.elsevier.com/locate/cej

Continuous hollow alumina gel fibers by direct electrospinning of an alkoxide-based precursor

Vasana Maneeratana, Wolfgang M. Sigmund *

University of Florida, Department of Materials Science & Engineering, P.O. Box 116400, Gainesville, FL 32611-6400, USA

Received 15 June 2007; received in revised form 2 September 2007; accepted 3 September 2007

Abstract

This work expands the field of view in ceramic fiber electrospinning, wherein ceramic fibers of hydrous alumina are directly electrospun from alkoxide-based precursors. The continuous fibrous bundles are produced with consistent tubular structures. The stability of the drawn fibers is dominated by the hydrolysis and condensation kinetics of the sol–gel precursor, which in parallel changes the processing parameter relationships found in traditional electrospinning. Here, we explore the nature and introduce the processing development of the sol–gel based fibers through electrospinning.

Keywords: Electrospinning; Alumina; Sol–gel; Macroporous ceramics; Fibers; Hollow fibers; Hollow tubes

1. Introduction

Thermal diffusivity, structural support, acoustic dampening, filtration, cell growth are some applications in which macroporous ceramics can be found. Macroporous ceramics incorporate, but are not limited to, pores on the order larger than 400 nm–4 mm [1]. With the growing needs for macroporous ceramics to push the envelope in various advanced applications such as high temperature filtration, insulation, and catalysis, the processing of such items need to provide the necessary corresponding microstructure in a more efficient and reliable manner. These porous bodies have been produced by various techniques ranging from sintering of simple porous powder compacts, replication, sacrificial templation, and direct foaming [1,2].

To add to the extensive latter-mentioned works, electrospinning has emerged as a novel bottom-up processing approach to fabricate micro and nanoscale fibers that can form dense ceramic fibrous structures [3]. As early as the late 1930s electrospinning was introduced as a method utilizing an electric field to rapidly draw fine streams of polymer fibers in a directed path; wherein this fine stream would result in rapid solvent evaporation and hence expedited fiber formation [4,5]. In the past decade, an extension of this technology into the field of ceramics evolved by incorporating ceramic particles and/or sol–gel precursors into polymer solutions; wherein the polymer matrix could be removed by simply calcining afterwards and the desired ceramic composition would remain [3].

This relative ease in ceramic electrospinning was counterbalanced by issues in both the precursor preparation realm due to sol–gel precursor/polymer miscibility and structural integrity issues during polymer calcination. Thin film recipes were modified to produce these predominant polymer precursors with minute concentrations of ceramic precursors. Before electrospinning was applied to ceramic fibers, ceramic fibers were melt-spun or solution-spun with high temperature melts or spinnable sols, respectively. In following the last decade, electrospinning has brought about less than a handful of researchers that have turned their attention to carefully preparing sols with spinnable viscosities to be used in electrospinning as opposed to the polymer dominated systems [6,7]. Successfully, the latter-mentioned works have produced a limited range of ceramic fiber compositions, including silica (SiO_2), alumina (Al_2O_3), and titania (TiO_2). The limitations involving spinnable sols reside in the fact that the relative solution viscosities are time and temperature dependent, but nonetheless provide a more reliable avenue to producing direct ceramic fibers through electrospinning.

Nonetheless an evolution has ensued in precursor development for a new type of ceramic precursor that would take into account all latter-mentioned issues: polymer miscibility issues, structural defects during calcination, and finally dependence

* Corresponding author.
E-mail address: wsigm@mse.ufl.edu (W.M. Sigmund).

1385-8947/$ – see front matter © 2007 Elsevier B.V. All rights reserved.
doi:10.1016/j.cej.2007.09.013

on gelation times to achieve spinnable viscosities. With our alkoxide-based precursor, continuous fibers can be directly fabricated through electrospinning efficiently than previously seen without the need for template burnout and time/temperature-dependence on viscosity [8]. Typical electrospinning parameters derived for both polymers and ceramics aim to predict fiber diameters by relating parameters such as flow rate, total current directed toward the lower electrode, surface tension, and for ceramics in particular, the solution conductivity [3,9–12]. Since our work departs from using a solution matrix dominated by a polymer, we needed to backpedal our understanding of basic electrospinning phenomena that can have an effect on the alkoxide-based fibers being produced [3].

Here, we explore the nature of the sol–gel based precursors in relation to typical electrospinning parameters to thereby form stable and continuous hydrous ceramic fibers with hollow characteristics.

2. Experimental

2.1. Preparation of precursors

Aluminum tri *sec* butoxide (ASB) was chosen as the main sol–gel alkoxide, >97%. These precursors were prepared with *sec* butyl alcohol (sBA), diethylene glycol monoethyl ether (DGME). Solutions were mixed in molar ratios (ASB:solvent). All solutions were obtained from Sigma–Aldrich.

2.2. Electrospinning

A vertically mounted apparatus was utilized with a Braintree Scientific, Inc. syringe pump, power source from Gamma High Voltage, Inc., 5 ml syringes from Becton-Dickinson, and disposable blunt-tip needles from Howard Electronics. The diameters of the blunt-tip needles were defined to be the inner diameters in millimeters (mm). The working distances were defined to be the distance from the end tip of the needle to the top of the grounded collection plate, which was comprised of aluminum foil. Electrospinning was performed in a fume hood with a range of relative humidity between 35 and 40% at 25 °C.

2.3. Flow rate study

The flow rate conditions were studied with a 5 cm^3 syringe and a 1.651 mm diameter disposable blunt-tip needle. The electric field was set at 10 kV and working distance of 15 cm. The flow rates that were studied ranged from 1.27 up to 17.8 cm^3/h. The solutions tested were comprised of ASB and sbA in ratios (ASB:sbA) of 1:1, 2:1, and 3:1. These tests were repeated to account for variability.

2.4. Change in precursor hydrolysis rate

DGME was added to ASB in the following ratios (ASB:DGME) of 1:1, 2:1, and 3:1. The reactions were performed in glass jars and stirred at room temperature. Duplicate solutions were also mixed to take into account variability. The above-mentioned flow rate protocol previously was utilized to analyze this study.

2.5. Scanning electron microscopy

Samples were mounted utilizing copper tapes on aluminum stubs. Samples were coated with Gold–Palladium. Both a JEOL 6335F and JEOL 6400 were utilized at 15 kV.

2.6. Fiber diameter analysis

The Carnoy 2.1 software was used to measure fibers captured in the SEM. Carnoy establishes a pixel to distance ratio, in which case, the cursor measures the scale bar at a particular distance and thus computes a ratio of micrometer (μm) per pixel. SEM images at 200× were analyzed, at least three images were taken per given condition, and fibers within the same depth of focus were measured. The limitations of the distance per pixel measured with 200× micrographs is within 1 μm, therefore measurements were recorded in μm to the corresponding whole number.

The data set comprised of recorded diameters, which was utilized to create a histogram to confirm single or multi-modal means and standard deviations per measured condition. In following, means and standard deviations were calculated per data set distribution. Afterwards the data was plotted and fit with both a Levenberg-Marquardt and Robust fitting to a Gaussian peak fit using the pro Fit 6.0.4 software. Chi-squared values were accepted for fittings of values less than 11 due to the wide range of possible fiber diameters. Once fitted means and standard deviations were computed, a probability density function (PDF) was graphed about the computed mean(s). The Gaussian PDF was calculated with the expected value to be the same as the mean and standard deviation calculated per data set distribution. A fitted curve is thus graphed with the calculated PDF. The corresponding graphs are a delineation of the probability of finding a certain fiber diameter with graphical axes of probability versus fiber diameter.

2.7. Effect of voltage, working distance, the electric field, and needle gauge

Solutions of the ASB:DGME system with a 2:1 molar ratio were electrospun at 10 kV at working distances of 10, 15, and 20 cm with a 7.62 cm^3/h flow rate. In addition samples were electrospun at 20 kV at 20 cm also with the same flow rate. Each of the parameters was tested with needle diameters of 1.245, 0.889, 0.711, and 0.556 mm.

3. Results/discussions

3.1. Precursor preparation

Typically in electrospinning, the spinnable solution is drawn by the electric field to the collection plate, wherein there will be a myriad of forces that balance to create a continuous jet. Important factors are conductivity along with viscosity in the balance, importantly solvent evaporation results in the contin-

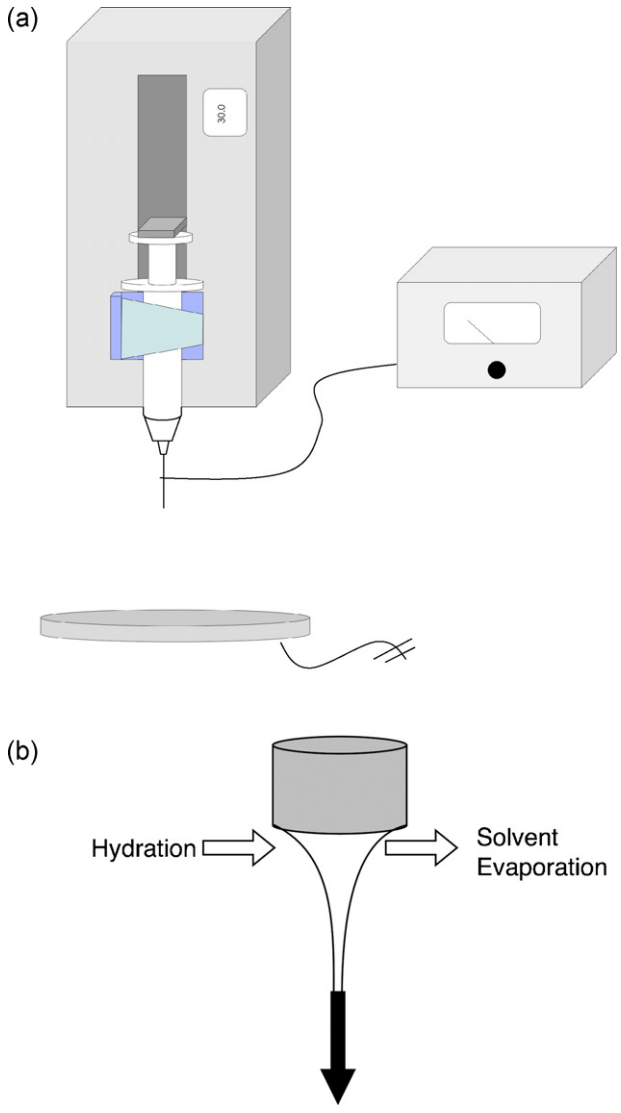

Fig. 1. (a) Electrospinning set up with syringe pump, power source, and grounded collector plate. (b) Schematic of the extrudate undergoing hydration and solvent evaporation at the nozzle's tip. The dark arrow illustrates the direction of the fiber drawing direction.

uous solidification of the fiber jet during the elongation of the fiber.

Meanwhile in this alkoxide-based solution system, the hydrolysis and condensation rate of the precursor is another extremely important factor that contributes to the stability of the drawn jet in parallel to the solvent evaporation. In Fig. 1a, the typical electrospinning set up can be seen. In addition to the latter, there is a schematic in Fig. 1b, illustrating the jet's dynamic hydrolysis and solvent evaporation at the tip of the nozzle. Typically in electrospinning polymers, (a) solvent(s) evaporate(s) as the jet is extruded and whipped onto the collection medium, resulting in solidified fibers [3,10,12]. In this work, solvent evaporation is also taking place, in addition to the driving force for the alkoxide to undergo hydrolysis and condensation. The latter propels the alkoxide to instantaneously react at the extrudate's surface thusly proceeding through the series of reactions of hydrolysis and condensation, as shown in Fig. 2, and forming the alumina gel structure. Forming of structures can be thought to result from the sol–gel species reacting out of solution and into polymerized gel structures. These condensates can form structures ranging from spheres, broken fibers, to hollow fibers. Further in this paper we will elucidate the relationship that electrospinning processing parameters have on fiber formation.

Current electrospinning methodologies producing hollow structures utilize a co-axial electrospinning technique, which involves concentric nozzles and/or heterogenous solvent mixtures [13–15]. Our technique differs since hollow fibers form without changes in the nozzle; in parallel there is a change in the immiscibility of the ceramic gel and any native alcohol present. Referring back to the electrohydrodynamic atomization theory (EHDA), a radial profile of the axial liquid velocity can be ascribed for the jet [10,16]. Therefore in addition to the latter-mentioned phenomenon, it is our current hypothesis that hollow structures can be formed by the combination of the radial profile of the axial liquid velocity and the instantaneous reaction at the extrudate surface which then results in a series of reactions from the outside wall inward. This outside-in hydrolysis/condensation reaction gradient thus can result in the hollow structure formation, once all metal-alkoxide is consumed.

Potentially these hydrated alumina fibers, or alumina gel fibers can be further processed for additional usage with thermal treatment studies. In following firing will allow a dehydration of the metal hydrate, which results in traditional ceramic compositions [8,17].

3.2. Flow rate study

This dynamic relationship of the hydrolysis/condensation and solvent evaporation was studied by understanding the flow rate effect on the formation of fibers. Three solutions of the ASB:sBA system were initially tested, with molar ratios of 3:1, 2:1, and 1:1. The flow rate was chosen as the initial field to test because the flow rate directly determines the time of exposure of the precursor to the atmosphere and hence the hydrolysis/condensation and solvent evaporation times. The solvent ratio was also varied in parallel to examine the concentration threshold for maximum solvent evaporation to continuously form fibers.

At the largest solvent concentration of 1:1, there were no fibers produced with any of the flow rate conditions. Nonethe-

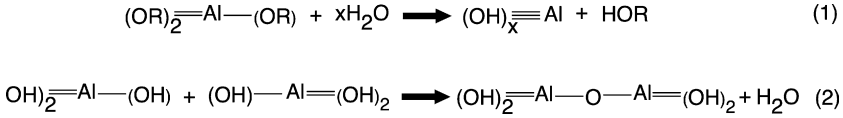

Fig. 2. Reaction set for typical aluminum alkoxides. (1) Hydrolysis is a results of an alcoholysis of the alkoxide (OR) and hydroxy group forming ligand. (2) Condensation is a result of a combination of hydrated ligands coming to form oxygen to metal to oxygen linkages, resulting in water, as a by-product.

less particles, particularly hollow particles, were formed that ranged in size dispersity depending on the flow rate as shown in Fig. 3a–d. At this current solvent concentration, it is hypothesized that the hydrolysis and condensation still yields solid structures, wherein the large concentration of the solvent leads to discontinuous stabilization of the jet walls, better known as varicose instability as described by the EHDA theory. This break up of the jet thus can drive particles to form as the most thermodynamically stable shape.

Meanwhile the 3:1 solutions demonstrated that continuous hollow fibers could be formed above 6.35 cm^3/h. However at flow rate values above 12.70 cm^3/h, continuous fibers were ill formed due to a lack of adequate solvent evaporation, which resulted in the bundles congealing. At low flow rate values, less than 2.57 cm^3/h, dried hydrous alumina globules were collected wherein there was often solidification of the precursor at the needle tip, as seen in Fig. 2a. These low flow rate structures differ from those found with the higher concentration of solvent, possibly due to the rapid drying. This rapid drying may form skins that dry before the rest of the body can react, resulting in incongruous drying. However between 2.54 and 6.35 cm^3/h, partial hollow structures were formed, characterized by some rods, malformed fibers, particles, and globules, as seen in Fig. 2c. The latter is an indication that the rate of drawing out the alkoxide can increase the possibility of forming stabilized fibrous walls to lead to continuous fiber formation. However there is still some varicose instability that can factor into this relationship, which produces the discontinuous and distorted fibers. Above 6.35 cm^3/h continuous bundles of tubular fibers formed, however the optimum range for fabrication of fibrous bundles with few deformed structures, such as particles, rods smaller than 200 micrometer were found between 7.62 and 11.43 cm^3/h for this particular ASB:sBa system, as seen in Fig. 2d.

The morphological difference between the 1:1 and 3:1 solutions may be a result of a critical concentration of hydrolyzed species necessary to form the stable jets and overcome varicose instability. Above this critical concentration of the ceramic precursor, the extrudate can undergo the necessary hydrolysis and condensation reactions that maintain the structural integrity of the jet for subsequent continual fiber drawing. The optimum flow rate values for 2:1 were similar as the 3:1 solution. Above and below this optimum flow rate resulted in the similar types of deformed structures. As a result of using a lower concentration precursor of 2:1 at optimal flow rates, there was a higher density of deformed or discontinuous structures found within the bundles. These continuous bundles were comprised of a presence of shorter fiber lengths overall when compared to the 3:1 batch. The latter reiterates the idea that at a certain threshold

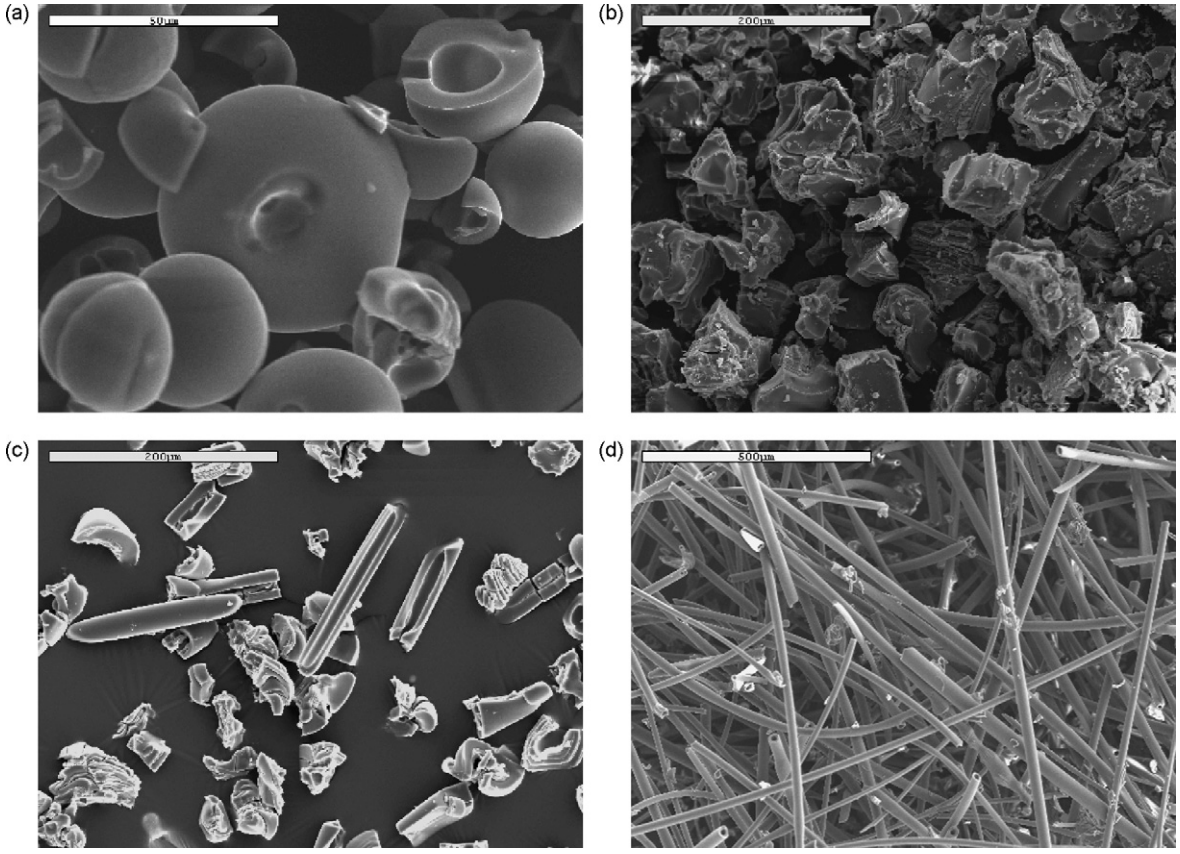

Fig. 3. Flow rate relationship for electrospun ASB:sBa solutions: (a) hollow particles produced with a 1:1 solution at 5.09 cm^3/h, 10 kV, 15 cm, and 0.712 mm needle gauge with scale-bar set at 50 μm; (b) globules produced from a 3:1 solution at a low flow rate of 2.57 cm^3/h, 10 kV, 15 cm, and 0.711 mm needle gauge with scale-bar set at 200 μm; (c) partial fibers and other deformed structures produced from a 3:1 solution at a moderate paced flow rate of 5.05 cm^3/h, 10 kV, 15 cm, and 0.712 mm needle gauge with scale-bar set at 200 μm; (d) bundle of fibers produced from a 3:1 solution at a flow rate of 5.05 cm^3/h, 10 kV, 15 cm, and 0.712 mm needle with scale-bar set at 200 μm.

concentration of alkoxide, such as 3:1, a consistent distribution of continuous hydrolyzed fibers can be produced.

3.3. Change in precursor hydrolysis rate

The role of another type of solvent can change the hydrolysis kinetics. This change is brought on thereby an alcoholysis, wherein certain added solvents, such as glycol ethers will lead to the ligand removal and subsequently substitution of the current alkoxide ligand (i.e. *sec*-butoxide). This case studied the effect of utilizing a glycol ether, specifically DGME. DGME serves two purposes; it serves as a higher boiling solvent and also has been used in the synthesis of metastable phases of alumina and also a lower alpha transition temperature [18]. In following with the flow rate study, it was found that the optimum flow rate ranges for the ASB:DGME with a 2:1 molar ratio proved to provide more consistent fibrous bundles with an optimum flow rate range of 6.35–10.16 cm^3/h. The fibrous bundles were similar in appearance as predominantly tubular.

Results for the 3:1 in a flow rate study showed that it was more difficult to consistently form fibers due to the excess solidification at the nozzle tip. Nonetheless fibrous bundles were formed in faster flow rate ranges of 7.62–12.70 cm^3/h. It was found that defected structures were often detected due to inconsistent fiber formation related to the excessive solidification at the tip resulting from inconsistent jet formation and stabilization. Wherein at the 1:1, particles were also formed that resembled the structures found with the ASB:sBA 1:1 system. This latter-mentioned inconsistency relates back the alkoxide precursor to solvent concentration. As the alkoxide flows, there must be enough solvent to allow flow and simultaneous hydrolysis for the stabilization of the jet, similarly the ASB:DGME 3:1 system lacked enough solvent to allow consistent flow and formation. Therefore with the addition of DGME, we find that the threshold for consistent fiber formation is within the 2:1 ratio as seen in Fig. 4. Since the hydrolysis of the DGME system is slower than the sBA system, slightly slower flow rates ranges provides an adequate amount of time for the stable jet to form, along with the use of a solution with more solvent concentration.

3.4. Effect of voltage, working distance and the electric field

Vital to electrospinning is the understanding the interplay of the electric field, which is thus studied by the ratio of the voltage to working distance (kV/cm). This electric field is denoted as the force responsible for creating the jet and stretching it down into a whipping motion until it deposits onto the grounded surface [3,9,12,16,19]. However since the dynamic interplay between the hydrolysis and solvent evaporation kinetics adds a new dimension, the electric field has been studied in two ways. The first is to understand the effect the electric field has on the mean fiber diameter. Another study investigates the same electric field values but at different working distances to contrast any inconsistencies that may be a result to the role of hydrolysis and solvent evaporation.

A probability density function was used to denote apparent probabilities versus fiber diameters, since variances are common for fiber diameters and it was more descriptive to show the distribution as an inclusive curve rather than point or bars with error bars, respectively. Some measurements resulted in PDF's with bi and at times tri-modal distributions (Fig. 5).

Within the same needle gauge, there were no apparent trends in the mean fiber diameters that were calculated with the electric fields of 0.5, 0.667, and 1.0 kV/cm. Fig. 5a and b, illustrates the probability distribution functions with needle diameters of 1.245 and 0.712 mm, respectively. There is an independent nature of the fiber diameter relative to the electric field, which lends itself to the dynamic yet currently unpredictable set of hydrolysis and condensation reactions taking place. This opposes previous studies that relate the inverse relationship of the electric field to ceramic fiber diameters [3]. However when looking at working distances, we come to understand this distance is necessary for solvent evaporation together with hydrolysis. Therefore the second part of this study compares the same electric field, 1.0 kV/cm, but set different working distances as seen in Fig. 5 and d. Fig. 5 is the PDF for various needle gauges at 1.0 kV/cm at 10 cm and Fig. 5 shows 1.0 kV/cm at 20 cm.

The PDF for the same electric field values show a very different trend, as seen in Fig. 5 and d. The distance at 20 cm demonstrated that fibers with smaller mean diameters could be produced at a high probability than those found at 10 cm. It was observed that the samples electrospun in the 10 cm working distance deposited smaller bundle sizes overall. Some

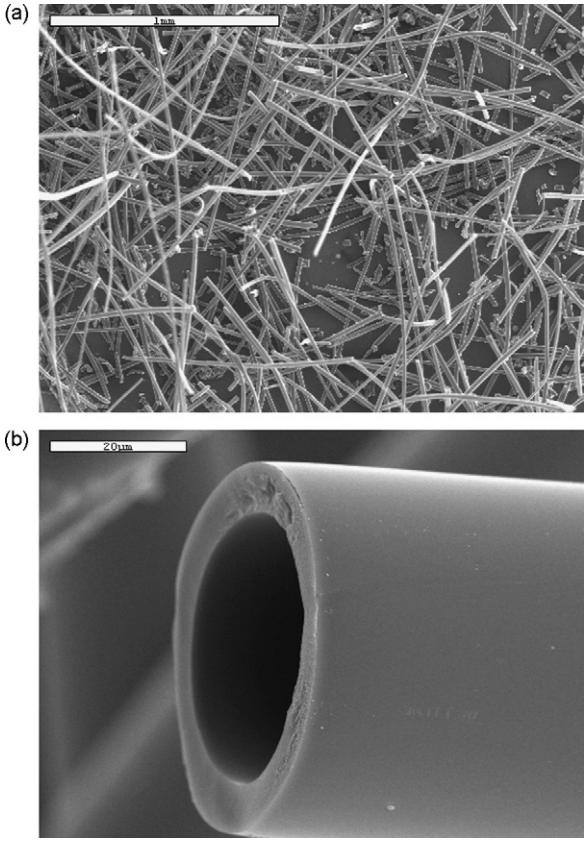

Fig. 4. Fibers formed with the 2:1 ASB:DGME solutions with parameters of 6.35 cm^3/h, 10 kV, 15 cm, and 0.712 mm needle gauge. (a) Fibrous bundle with scale-bar set at 1 mm and (b) end of hollow fiber with scale-bar set at 20 μm.

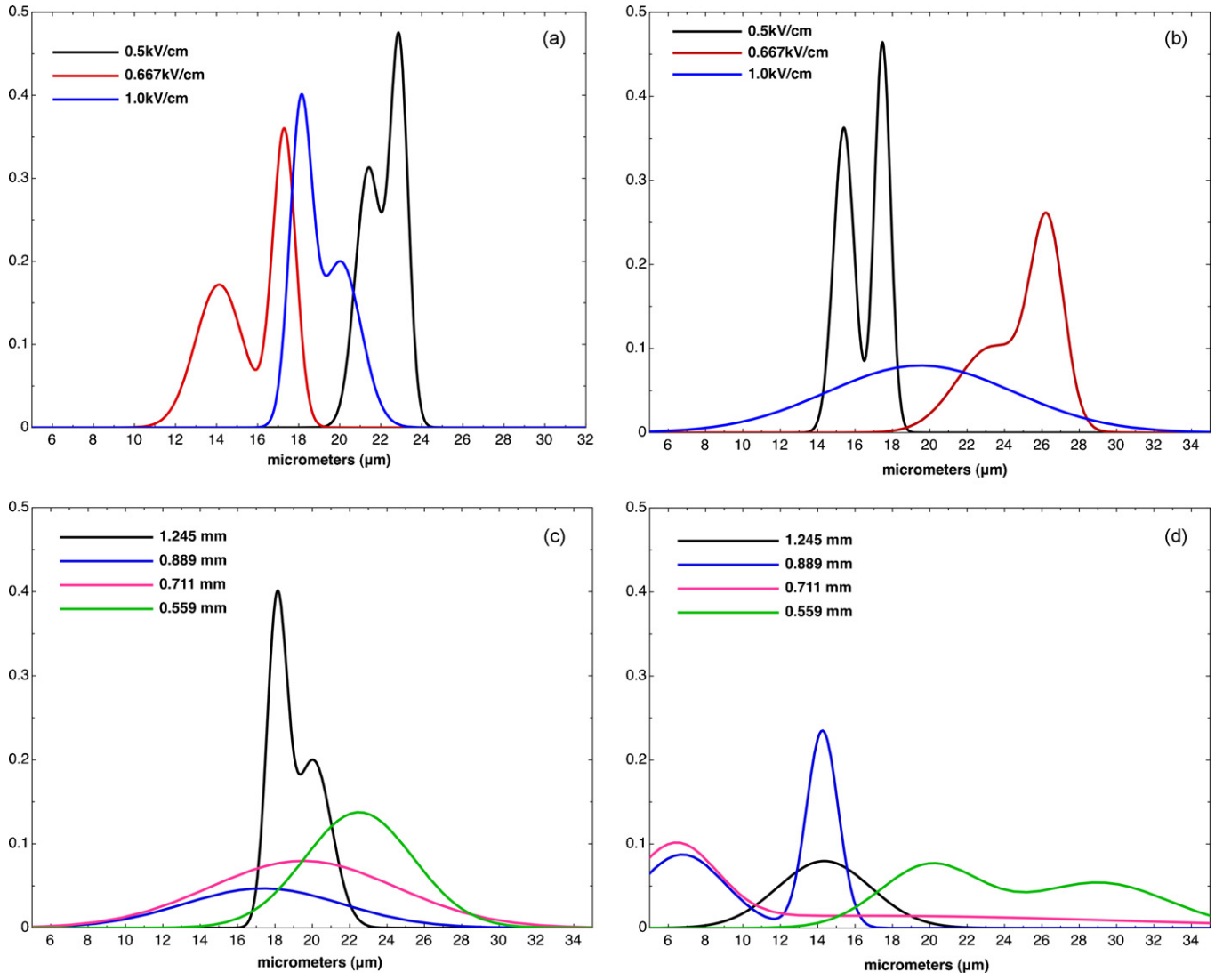

Fig. 5. (a) Comparison at various electric fields with needle diameter of 1.245 mm and 7.62 cm^3/h flow rate; (b) comparison at various electric fields with needle diameter of 0.712 mm and 7.62 cm^3/h flow rate; (c) PDF of 1.0 kV/cm at 10 cm and 7.62 cm^3/h flow rate; (d) PDF of 1.0 kV/cm at 20 cm and 7.62 cm^3/h flow rate.

congealing or collapse of the tubular structures was found in some bundles, which lead to fibers that could not be adequately measured.

However the 20 cm bundles produced fibers with little defects that were extremely elongated with no apparent signs of wetting. However, the fiber distribution is vast and this may be related to some of the jet splitting that is observed during the electrospinning process. As observed, before the whipping occurs, there is some splitting of the jet; this may be attributed to the inconsistent jet hydrolysis and condensation, which may solidify in a way to lead to the fiber division. Consequently the electric field is not a parameter that can dutifully predict the mean fiber diameters of our system, but can be used to decipher a range of fibers being fabricated as seen in the PDF's. In addition we see that the electric field is also not independent of the working distance due to the factors related to the hydrolysis and solvent evaporation in the stabilization of the jet and that a larger working distance can yield a range of fiber diameters that include much smaller fiber diameters, even less than 6 (μm).

3.5. Needle gauge

In parallel to the investigation performed with various needle gauges at the same electric field, as seen in Fig. 5c and d, there were studies performed at the 0.5 and 0.667 kV/cm (not shown) that wholly demonstrate a lack of trend of the fiber diameter mean or distribution relative to the needle gauge. Although previous studies have shown no relationship of the needle gauge in the polymer electrospinning condition [20], this sol–gel based system is dependent on exposure to atmospheric hydrolysis. Therefore the needle gauge relates to the reaction surface of the solution. However the size range of the nozzle may be at the critical size in which solidification thereby hydrolysis occurs, which can still lead to a stable jet.

4. Conclusions

The direct approach to fabricating continuous hollow fibrous alumina can thereby bring about new and fascinating avenues

to fabricate ceramic fibers for various applications that require faster electrospinning rates, structural integrity after firing, near-net shape after firing and also lack of impurities from additives. These bundles of tubular ceramics offer a new avenue in the world of macroporous materials, thereby opening avenues for new types of lightweight insulation. In this development, alkoxide-based solutions established the backbone of this work, wherein the utilization of the hydrolysis and condensation kinetics allowed for stabilization of the jet and hence continuous fiber formation. Processing parameters important to the traditional electrospinning system do not follow the same relationship with these precursor solutions, but only assist us in understanding optimal processing parameters for future works regarding direct ceramic fiber electrospinning. It is the hope of the authors that this work bridges the fields of traditional ceramic electrospinning with a new light thereby bringing about new and exciting compositions along with applications.

Acknowledgements

The authors acknowledge funding from the NASA Harriett G. Jenkins Predoctoral Fellowship Program for Ms. Maneeratana. Also the authors would like to acknowledge the Major Analytical Instrumentation Center at the University of Florida for access to the characterization facilities.

References

[1] A.R. Studart, U.T. Gonzenbach, E. Tervoort, L.J. Gauckler, J. Am. Ceram. Soc. 89 (2006) 1771–1789.
[2] P. Colombo, Philos. Trans. R. Soc. A Math. Phys. Eng. Sci. 364 (2006) 109–124.
[3] W. Sigmund, J. Yuh, H. Park, V. Maneeratana, G. Pyrgiotakis, A. Daga, J. Taylor, J.C. Nino, J. Am. Ceram. Soc. 89 (2006) 395–407.
[4] A. Formhals, Apparatus for Preparing Artificial Threads, US Patent 1,975,504 (1934).
[5] A. Formhals, Production of Artificial Fibers, US Patent 2,077,373 (1937).
[6] R. Riedel, E. Horvath-Bordon, S. Nahar-Borchert, E. Kroke, Adv. Ceram. Compos. 247 (2003) 121–128.
[7] W.K. Son, D. Cho, W.H. Park, Nanotechnology 17 (2006) 439–443.
[8] V. Maneeratana, W.M. Sigmund, Electrospun structures with controlled porosity and specific surface areas, in: Proceedings of the International Astronautical Congress, IAC-06-C02.04.07, International Astronautical Federation, Valencia, Spain, 2006.
[9] S.V. Fridrikh, J.H. Yu, M.P. Brenner, G.C. Rutledge, Polym. Nanofibers 918 (2006) 36–55.
[10] R.P.A. Hartman, D.J. Brunner, D.M.A. Camelot, J.C.M. Marijnissen, B. Scarlett, J. Aerosol Sci. 30 (1999) 823–849.
[11] J.M. Deitzel, C. Krauthauser, D. Harris, C. Pergantis, J. Kleinmeyer, Polym. Nanofibers 918 (2006) 56–73.
[12] S.A. Theron, E. Zussman, A.L. Yarin, Polymer 45 (2004) 2017–2030.
[13] J.T. Mccann, M. Marquez, Y.N. Xia, Nano Lett. 6 (2006) 2868–2872.
[14] P. Gupta, G.L. Wilkes, Polym. Nanofibers 918 (2006) 74–90.
[15] A.V. Bazilevsky, A.L. Yarin, C.M. Megaridis, Langmuir 23 (2007) 2311–2314.
[16] R.P.A. Hartman, J.P. Borra, D.J. Brunner, J.C.M. Marijnissen, B. Scarlett, J. Electrostat. 47 (1999) 143–170.
[17] V. Maneeratana, W. Sigmund, Property comparisons of direct electrospun alumina ceramic fibers, in: 10th International Conference and Exhibition of the European Ceramic Society, Berlin, Germany, J. Eur. Ceram. Soc. (2007).
[18] N. Bahlawane, T. Watanabe, J. Am. Ceram. Soc. 83 (2000) 2324–2326.
[19] R.P.A. Hartman, D.J. Brunner, D.M.A. Camelot, J.C.M. Marijnissen, B. Scarlett, J. Aerosol Sci. 31 (2000) 65–95.
[20] J. Macossay, A. Marruffo, R. Rincon, T. Eubanks, A. Kuang, Polym. Adv. Technol. 18 (2007) 180–183.